J Electr Eng Technol.2015;10(1): 205-215
http://dx.doi.org/10.5370/JEET.2015.10.1.205

ISSN(Print) 1975-0102
ISSN(Online) 2093-7423

Common Model EMI Prediction in Motor Drive System for Electric Vehicle Application

Yong-Ming Yang†, He-Meng Peng* and Quan-Di Wang*

Abstract – Common mode (CM) conducted interference are predicted and compared with experiments in a motor drive system of Electric vehicles in this study. The prediction model considers each part as an equivalent circuit model which is represented by lumped parameters and proposes the parameter extraction method. For the modeling of the inverter, a concentrated and equivalent method is used to process synthetically the CM interference source and the stray capacitance. For the parameter extraction in the power line model, a computation method that combines analytical method and finite element method is used. The modeling of the motor is based on measured date of the impedance and vector fitting technique. It is shown that the parasitic currents and interference voltage in the system can be simulated in the different parts of the prediction model in the conducted frequency range (150 kHz-30 MHz). Experiments have successfully confirmed that the approach is effective.

Keywords: Electric vehicles, Electromagnetic interference, Motor drives; Modeling, Parameter extraction

1. Introduction

Electric vehicles (EVs) are being actively research and development in recent years because they are an important way to deal with global environmental problems like global warming. EVs are characterized by motor drive systems, where electric power conversion is done by pulse width modulation (PWM) inverters [1-3].

The PWM technique provides high control efficiency and can be easily implemented based on the modern integrated circuit. Nevertheless the fast rise time of the switching transient produce high-frequency common mode (CM) electromagnetic interference (EMI) which leads to several serious problems such as CM current flowing to the ground through the stay capacitance of the system, shaft voltage and bearing current in motor, deterioration of motor winding insulation, radiation of power line, etc [4-6]. The problems of EMI may affect work state of motor drive systems and their surrounding electric device [7] and these highly concern the safety of EVs. Therefore, it is necessary to establish an accurate CM conducted EMI model for evaluating the level of the CM EMI in the motor drive system. Researchers have conducted a number of EMI modeling studies on the motor drive system of EVs [8-10] and other industrial applications [11-15]. A piece-wise linear insulated gate bipolar transistor (IGBT) behavior model for frequency simulation of motor drive EMI prediction have been proposed [16]. The inverter model is composed of a control circuit and a three-phase IGBT module with parameters extracted from different device measurement. However, the control circuit and test procedure are complex. A physics-based high-frequency model of power inverter including the IGBT unit cells, heat sink and connective printed circuit board (PCB) traces combined in a single electrical circuit is presented [17]. The IGBT model includes the high-frequency stray component superimposed on the well-known Hefner IGBT model and the components is calculated using a 3-D quasi-static finite element analysis. The invert model by this method is relatively accurate. Nevertheless, the geometric dimensions and the structural physical parameters of the IGBT have to be known first. A high-frequency modeling method, which takes into account phenomena such as skin effects, proximity effects and dielectric losses, is used to model power cables by the series association of n identical RLCG basic cells [18]. The parameter values in the model are obtained by measurement and specific date processing. Other Studies have adopted a four-port impedance matrix representation of the power line considered in CM and the impedance parameters value have been practically measured in various conditions by considering the relationship between the voltage and current of the ports [19]. However, the obtained deviation of the model by the two mentioned methods is depended on the measurement accuracy. A lumped RLC circuit is used to model a motor in the frequency range under 1 MHz [20]. The parameters in the model include the winding-to-frame capacitance, winding-to-rotor capacitance and phase leakage inductance. The authors give a behavior model of AC motor [21]. The asymptotical and analytical methods are proposed to model the AC motor. Other alternative method [22] is proposed, including a finite element analysis [23]. However, with the

† Corresponding Author: School of Electrical Engineering, Chongqing University, Chongqing, P. R. China. (yangyym@cqu.edu.cn)
* School of Electrical Engineering, Chongqing University, Chongqing, P. R. China. (penghemengok@163.com, wangquandi@cqu.edu.cn)
Received: March 14, 2014; Accepted: August 24, 2014

frequency increasing above 1 MHz, all these methods are no longer suitable because of low accuracy.

This study aims to establish a prediction model of CM conducted interference for motor drive system of EVs. The high-frequency CM models of various parts of the system are proposed. First, the inverter model is presented. To model the inverter, a stray capacitor representing capacitive coupling between the IGBT and the heatsink and a CM voltage source, which takes into account the feature information of multiple interference sources, are used. This concentrated and equivalent method on the inverter can reduce the complexity of calculation simulation and it is easy to establish the model by experimental measurement. Second, a high-frequency CM model of the power line in EVs, using distributed parameter circuits calculated by combining the analytical method and finite element method (FEM), is detailed. This method can avoid the derivations error generated from measurements, however, the power line structures and parameters must be given at first. Third, a new approach based on vector fitting [24] is proposed to model a motor from 150 kHz to 30 MHz by using measured impedance date. Compared with the general modeling methods, this approach have a higher accuracy in a wide frequency range. At last, it will be shown that CM current and voltage can be predicted with a satisfactory accuracy using the proposed method.

2. Study System

The studied system (Fig. 1) is a motor drive system for EV applications. It is constituted of a direct current power supply, an industrial LISN, a three-phase IGBT inverter, a permanent magnet synchronous motor (PMSM), and a three-phase power line connecting the inverter to the motor. The complete system is placed on a copper plane to enable the EMI noise to circulate.

Interference or noise flowing through heatsink, cable shielding layer, motor chassis and common ground is referred to as CM EMI. Note that in this study, only CM effects are considered, due to their dominant effects in

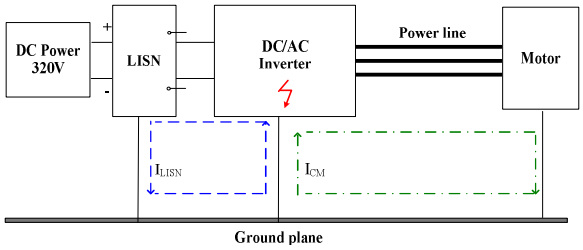

Fig. 1. DC/AC converter system with CM current pathways

EMI. Fig. 1 shows the CM current paths (I_{LISN} and I_{CM}) of the system with the noise source located in the main circuit. The CM currents exist because the sum of three instantaneous voltages at the output of the inverter is not null and capacitive couplings to ground are distributed in the complete system.

3. Modeling

The aim of the modeling is to predict conducted emissions in a variable-speed drive system. The essential question that needs to solve in CM modeling is obtaining the equivalent circuit parameters of each part in the CM conducted EMI propagation paths. Fig. 2 shows a simplified lumped element representation of the system. The CM equivalent circuits of the motor and power line need be precisely represented because these impedances have a significant influence on the level of conducted disturbances. The CM voltage source generated by the inverter should be carefully considered because the source is the reflex of the original EMI characteristics level in a system. In the following sections, we present several subsystem CM circuit models, such as the LISN model, inverter model, power line model, and motor model.

3.1 LISN Model

LISN is an industrial element for measuring the conducted interference in EMC standards. The parameters of the LISN circuit topology are provided by the

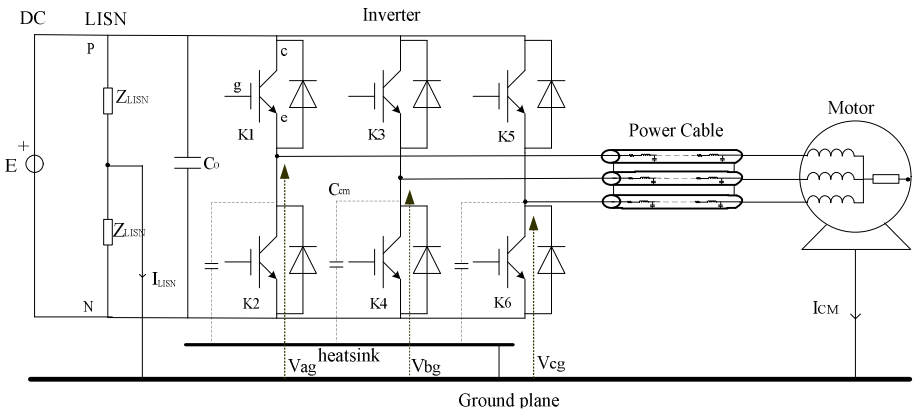

Fig. 2. Lump element equivalent circuit of the system

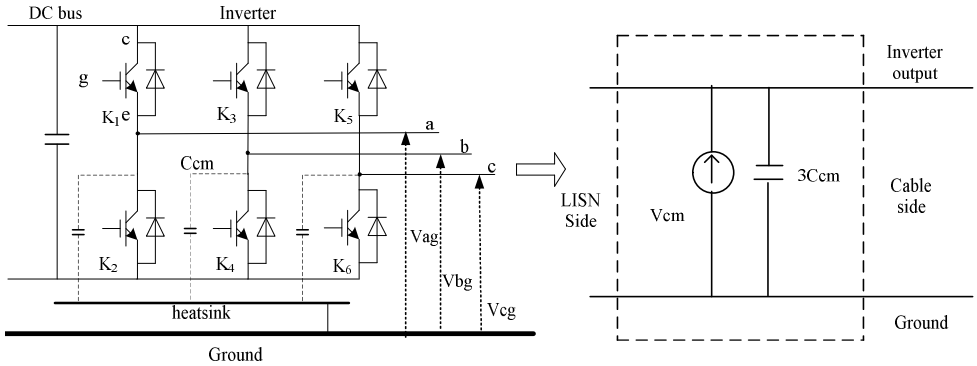

Fig. 3. CM equivalent model of the inverter

manufacturers. In this study, LISN is located between a power supply and inverter for three functions: Firstly, to prevent incoming conducted disturbance from the power supply. Secondly, to maintain the stabilized impedance 50 ohms at the power electronics converter terminal in the wide frequency range, and finally to couple conducted interference voltage signal from the converter to the measuring receiver.

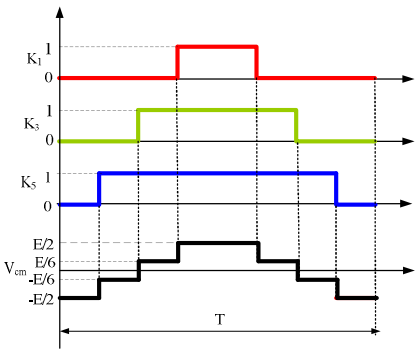

(a) SVPWM modulation signal and common model voltage

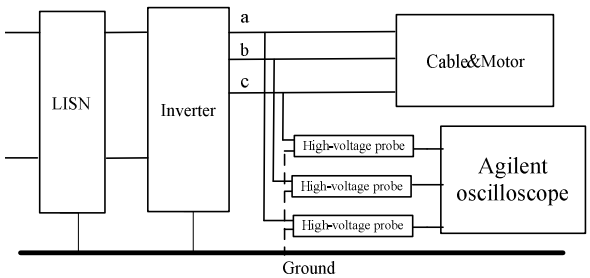

(b) V_{ag}, V_{bg}, and V_{cg} voltages acquisition setup

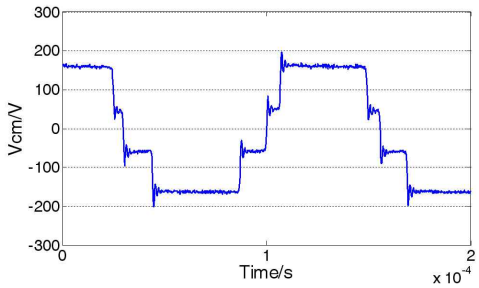

(c) EMI source waveform

3.2 Inverter model

Fig. 3 shows the inverter stage with the main stray capacitor C_{cm} representing capacitive coupling between the IGBT and the heatsink, and the voltages V_{ag}, V_{bg} and V_{cg} which are the output voltages of a leg of the inverter referenced to ground. In the common mode, the three inverter legs, generating the CM interference voltage, can be considered as a single voltage source V_{cm}. The model of V_{cm} and C_{cm} are presented in the following parts.

3.2.1 CM *voltage source model*

CM voltage generated by the inverter is expressed as

$$V_{cm} = 1/3(V_{ag} + V_{bg} + V_{cg}) \quad (1)$$

The system of impedances Z_{LISN} constitutes a voltage divider, which makes the point ***P*** and ***N*** (Fig. 2) on the DC source have the voltage potential of 1/2E and -1/2E,

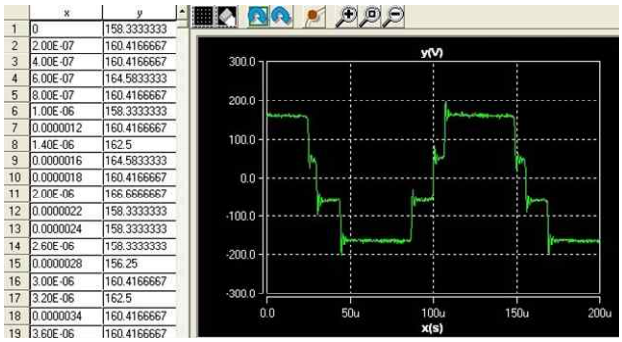

(d) Measured wave is imported to the model

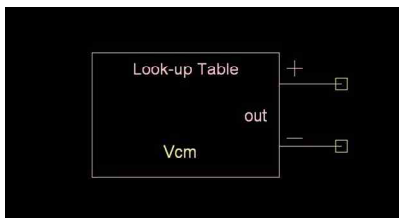

(e) Model established by MAST language

Fig.4. CM voltage source modeling process

respectively. As a space vector pulse width modulation (SVPWM) method is used in this system with the regulated DC source voltage E, the turn on signals of the higher transistors (K_1, K_3, K_5) are shown as Fig. 4(a). Each voltage (V_{ag}, V_{bg} and V_{cg}) has the value of 1/2E when the higher transistors are turned on, and -1/2E when the lower transistors (K_2, K_4, K_6) are turned on. Then, substituting each voltage (E/2 or –E/2) into (1), the CM voltage V_{cm} is illustrated as Fig. 4(a). It can be observed that the voltage step of V_{cm} caused by the on/off of the switches are ±1/3E at every switching transient and this stairway voltage is particularly perturbing because it is constituted by six transients (dv/dt) per period.

An electric vehicle industrial inverter supplied by the DC power source has been used in our experiments, its switching frequency was 7.5 kHz, and SVPWM strategy is used to generate the output voltages. The output voltages V_{ag}, V_{bg} and V_{cg} are experimentally determined by using an Agilent oscilloscope and three Agilent high-voltage probes (Fig. 4(b)). Then, the CM voltage V_{cm} is obtained by the equation (1), as shown in Fig. 4(c).

The very essence of this modeling method for CM voltage source is that a stairway voltage is substituted for six switching elements by experimental measurements and subsequent calculations, and the characteristic of the CM EMI can be correctly described by the stairway voltage. Date from the CM voltage in Fig. 4(d) is stored in a memory module of simulation software where the date can be checked and edited. These data can be changed into a two-port model which represents the function of measured voltage through MAST language (Fig. 4(e)), then add the established model into component library. When building the CM conducted EMI circuit model of the variable-speed ac motor drive system in the simulation software, the established CM voltage source model should be invoked.

3.2.2 Parasitic parameter C_{cm} model

The capacitive coupling to ground in the converter is mainly due to the power module and its heat sink, as explained by the schematic representation of Fig. 5(a). As the heat sink is connected directly to ground, this capacitance is a propagation path for the CM current.

The value of C_{cm} (Fig. 5(b)) is determined using an impedance analyzer. The impedances Z_{ag}, Z_{bg}, and Z_{cg} are measured between each leg of the inverter and the ground as shown in Fig. 5(c). The measured impedances are capacitive until 25 MHz, beyond 25 MHz, turning to inductive because of parasitic inductance introduced during measurement. In fact, this inductance does not exist in the system, so it can be neglected. Therefore, Z_{ag}, Z_{bg}, and Z_{cg} are assimilated to an identical capacitance C_{cm} equal to 267 pF from 150 kHz to 30 MHz. The impedance frequency characteristics comparison of Z_{ag} and C_{cm} is illustrated in Fig. 5(d).

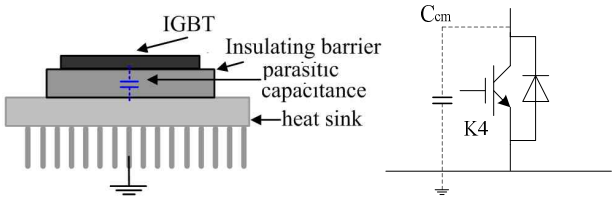

(a) Physical model (b) Circuit Model

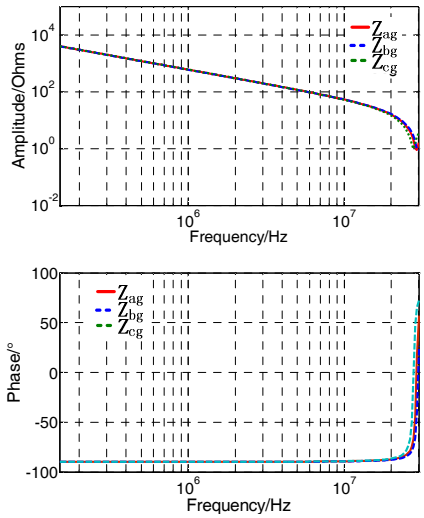

(c) Measurement impedance between each leg to the ground

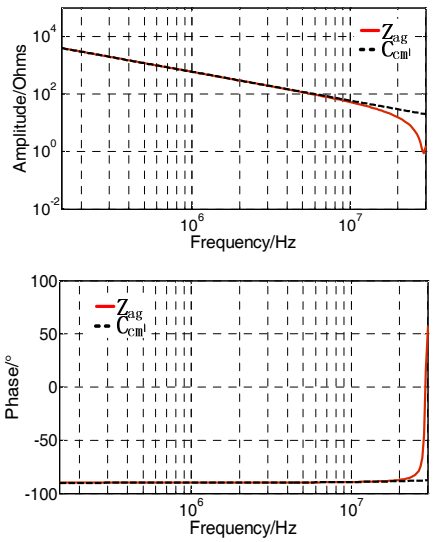

(d) The comparison between measurement impedance and equivalent parasitic parameter C_{cm}

Fig. 5. Parasitic parameter C_{cm} extraction process

3.3 Power line model

Power line spread paths of CM conducted disturbances in motor drive system. In order to predict the EMI level produced by the system, a high-frequency equivalent circuit model should be established for the power line.

Three cross-linked polyethylene insulated cables are

used in the study, the geometrical and physical parameters of single phase cable are shown in Fig. 6(a), the conductor of cable is composed of 19 bundle mutual insulation copper wires, therefore, the variation of inductance and resistance with frequency by skin effect is neglected here; the shielding layer is connected to both the heatsink of the inverter and the shell of the PMSM, space between the cables is 50mm.

A power line can be viewed as a three conductor transmission line guided by transmission line theory, Fig. 6(b) shows per meter length model of the power line. Mutual capacitance C_M of two conductors is considered to be zero in theory because of the shielding layer existing in each phase cable; and the value of mutual inductance L_M, which is much less than self inductance because the space between the cable is large, can be neglected. All conductors are considered in parallel for the CM current propagation paths in the power line and the power line CM model can be described as Fig. 6(c).

In this section, we have proposed power line CM model (Fig. 6(c)) obtained by the series-association of N identical RLC basic cells. The analytic method is applied to calculate both the resistance parameters and the inductance parameters and FEM is employed to determine the capacitance parameters.

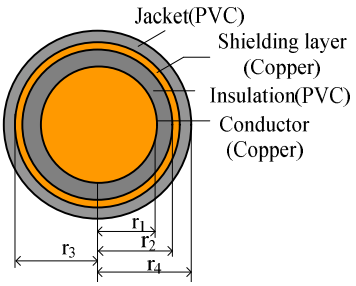

r_1	3.25mm
r_2	4.35mm
r_3	4.75mm
r_4	5.75mm
μ_0	1.26 10^{-6}H/m
μ_r	1
ε_0	8.85 10^{-12}F/m
ε_r	4.3
σ	58 MS/m
ρ	1.72 $10^{-8}\Omega$/m

(a) Geometrical and physical parameters of single phase cable

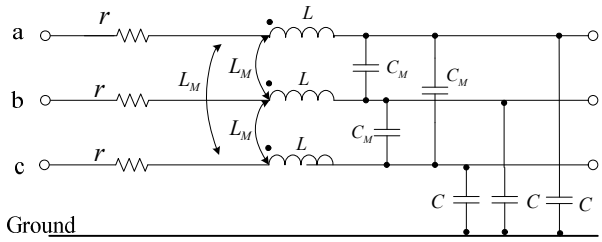

(b) Power line TLM model

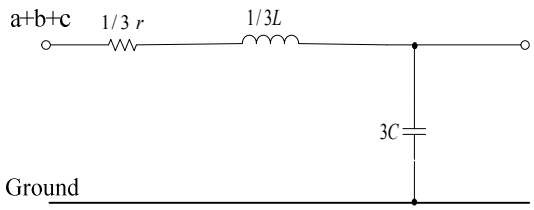

(c) Simplified power line CM model (per unit length)

Fig. 6. Power line CM model process

3.3.1 Inductance parameters

The analytic method model to calculate self-inductance of single cable is shown in Fig. 7. The outer conductor and inner conductor represent the conductor and the shielding layer of the cable, respectively, the outer conductor has negligible thickness, and the current is uniformly distributed inside the inner conductor.

The current density inside the inner conductor is

$$\boldsymbol{J}=\frac{I}{\pi a^2}\boldsymbol{e}_z \tag{2}$$

The magnetic flux density within the inner conductor at any radius ρ such that $0 \le \rho \le a$, from Ampere's law, is

$$\boldsymbol{B}_i=\frac{\mu_0 I\rho}{2\pi a^2}\boldsymbol{e}_\phi \tag{3}$$

The flux enclosed in the region between ρ and $\rho+d\rho$, the unit length in the z direction is

$$d\Phi_i=\frac{\mu_0 I}{2\pi a^2}\rho d\rho \tag{4}$$

As only a fraction of the total current is enclosed by the contour at radius ρ, the flux linkages are

$$d\psi_i=\frac{\mu_0 I}{2\pi a^4}\rho^3 d\rho \tag{5}$$

Thus, the total flux linkages within the inner conductor are

$$\psi_i=\frac{\mu_0 I}{2\pi a^4}\int_0^a \rho^3 d\rho=\frac{\mu_0 I}{8\pi} \tag{6}$$

Hence, the inductance per unit length of the inner

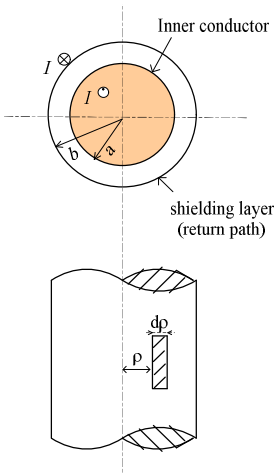

Fig. 7. Inductance parameters calculation model a=3.25 mm, b=4.55mm

conductor due to the flux inside it is

$$L_i = \frac{\psi_i}{I} = \frac{\mu_0}{8\pi} \quad H/m \tag{7}$$

Next, determine the inductance due to the flux between the two conductors. The flux density in the region $a \le \rho \le b$ is

$$\boldsymbol{B}_e = \frac{\mu_0 I}{2\pi\rho}\boldsymbol{e}_\phi \tag{8}$$

The flux passing through the region between ρ and $\rho + d\rho$, the unit length in the z direction is

$$d\Phi_e = \frac{\mu_0 I}{2\pi}\frac{1}{\rho}d\rho \tag{9}$$

The total flux linkages are

$$\psi_e = \frac{\mu_0 I}{2\pi\rho_4}\int_a^b \frac{1}{\rho}d\rho = \frac{\mu_0 I}{2\pi}\ln\frac{b}{a} \tag{10}$$

Thus, the contribution to the self-inductance by these flux linkages is

$$L_e = \frac{\psi_e}{I} = \frac{\mu_0}{2\pi}\ln\frac{b}{a} \quad \text{H/m} \tag{11}$$

In the region $b \le \rho$, the magnetic flux density is zero. Hence, the total inductance per unit length of the insulated cable is

$$L = L_i + L_e = \frac{\mu_0}{2\pi}(\frac{1}{4} + \ln\frac{b}{a}) \quad \text{H/m} \tag{12}$$

3.3.2 Capacitance parameters

For calculating the capacitance between the conductor and shielding layer, The FEM model of the phase cable is created in Maxwell 2D (Fig. 8). Calculating the capacitance from FEA is related to the electrostatic energy $\boldsymbol{W}^{\boldsymbol{C}}$. The first step is to assign a voltage U_1 to the conductor; the shielding layer in the volume V is grounded. FEA programme discretizes problem volume V into triquetrous element as shown in Fig. 8 and then solves the

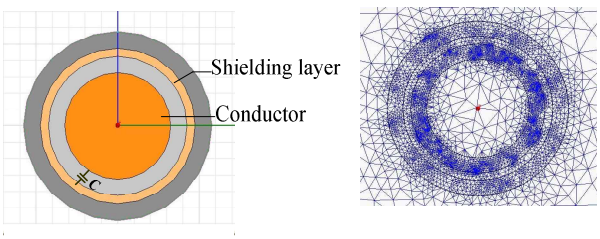

Fig. 8. FEM model for capacitance computation

Laplace equation to get the electric field $\boldsymbol{E}_1$ and the displacement field $\boldsymbol{D}_1$ according to (13).

$$\begin{aligned} &\nabla\cdot(\varepsilon\nabla\Phi_1) = 0 \\ &\boldsymbol{E}_1 = -\nabla\Phi_1 \\ &\boldsymbol{D}_1 = \varepsilon\boldsymbol{E}_1 \end{aligned} \tag{13}$$

Where, Φ_c is the electric scalar potential. The same procedure is applied to shielding layer in succession; in the end, $\boldsymbol{W}^{\boldsymbol{C}}_{12}$ which is stored in the electric field associated with the capacitance between the conductor and shielding layer can be obtained from (14).

$$W_{12}^C = \frac{1}{2}\int_V \boldsymbol{E}_1\cdot\boldsymbol{D}_2 dV = \frac{1}{2}\int_V \boldsymbol{E}_2\cdot\boldsymbol{D}_1 dV \tag{14}$$

Since the energy can also be expressed

$$W_{12}^C = \frac{1}{2}CU_1U_2 \tag{15}$$

Where C represents the capacitance between conductor and shielding layer, further combing the (14) and (15), we can get C as

$$C = \frac{\int_V \mathrm{E}\cdot\mathrm{D}dV}{U_1U_2} \tag{16}$$

3.3.3 Resistance parameters

The resistance parameters of the per-unit-length conductor are defined as

$$r = \frac{1}{\sigma S} = \frac{1}{\sigma\pi r_1^2} \tag{17}$$

The RLC parameters of the EMI model of the power line are computed using the aforementioned setup, and the equivalent circuit model of the per-unit-length power line (1m) is shown in Fig. 9.

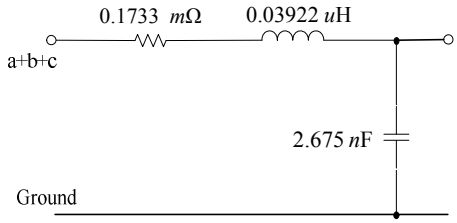

Fig. 9. CM Equivalent circuit of the power line

3.4 Motor model

PMSM is a main propagation path for CM conducted emission of the drive system. In order to predict the EMI level, a high-frequency equivalent circuit model should be

established for the motor. In this section, vector fitting (VF) method is proposed to model the PMSM with high accuracy from 150 kHz to 30 MHz, using measured impedance date.

3.4.1 Vector fitting technique

Vector fitting [24] is widely used for fitting a rational function for frequency domain response; it also is an accurate, robust, and efficient method. By applying vector fitting, the rational function of motor obtained by experimental date can be approximated a transfer function $f(s)$ as

$$f(s) \approx d + se + \sum_{k=1}^{N} \frac{r_k}{s - p_k} \tag{18}$$

The terms r_k and p_k are the residues and poles, respectively, they could be real or complex conjugate pairs while d and e are real. In this paper, s is equivalent to $j\cdot\omega$ for motor impedance application where ω is the angular frequency.

Then, we convert the rational approximation given by (18) into an equivalent circuit using in simulating software. It can be divided into several sub-circuits in terms of the order of the function as follows.

1) Equivalent circuit for *d* and *e*

A *RL* series circuit (Fig. 10(a)) will be used to synthesize the parameters d and e in function *f(s)*. The values of R and L are

$$R = d; \quad L = e \tag{19}$$

2) Equivalent circuit for real poles

The impedance rational expression for a real pole and residue is

$$f(s) = \frac{r_{kr}}{s - p_{kr}} \tag{20}$$

A simple *RC* parallel circuit (Fig. 10(b)) is used to replace the rational function with one real pole. Comparing the circuit impedance with (20), the values of R and C are

$$R = -\frac{r_{kr}}{p_{kr}}; \quad C = \frac{1}{r_{kr}} \tag{21}$$

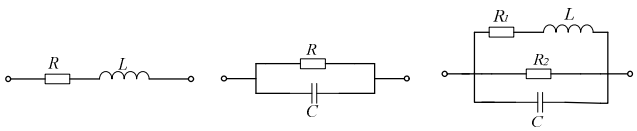

(a) RL circuit (b) RC circuit (c) RLC circuit

Fig. 10. Equivalent circuit

3) Equivalent circuit for a complex conjugate pole pair

The complex conjugate pole pair can be expressed by the impedance rational as

$$f(s) = \frac{r_{kc}}{s - p_{kc}} + \frac{r_{kc}^*}{s - p_{kc}^*} \tag{22}$$

Where p_{kc} and p_{kc}^* are complex conjugate pole pair and r_{kc} and r_{kc}^* are the residue pair. The equivalent circuit composed of *RLC* for representing (22) is shown in Fig. 10(c) and the values of these parameters are

$$\begin{aligned}
C &= \frac{1}{r_{kc} + r_{kc}^*} \\
L &= \frac{r_{kc} + r_{kc}^*}{p_{kc} p_{kc}^* + \left[-(p_{kc} + p_{kc}^*) + \frac{r_{kc} p_{kc}^* + p_{kc} r_{kc}^*}{r_{kc} + r_{kc}^*} \right] \frac{r_{kc} p_{kc}^* + p_{kc} r_{kc}^*}{r_{kc} + r_{kc}^*}} \\
R_1 &= -\frac{L(r_{kc} p_{kc}^* + p_{kc} r_{kc}^*)}{r_{kc} + r_{kc}^*} \\
R_2 &= \frac{r_{kc} + r_{kc}^*}{-(p_{kc} + p_{kc}^*) + \frac{r_{kc} p_{kc}^* + p_{kc} r_{kc}^*}{r_{kc} + r_{kc}^*}}
\end{aligned} \tag{23}$$

With the sub-circuits obtained above, the total impedance of *f(s)* is represented by connecting sub-circuits in series.

3.4.2 CM impedance measurement and modeling

For the CM conducted emission of the system, the three phases of the motor are considered in parallel and the CM parameters of motor (Z_{CM}) are identified by inspecting the input impedance measured between the motor three phase winding connected together and the motor frame, as shown in Fig. 11. The CM impedance is obtained by using an impedance analyzer in the frequency range from 150 kHz to 30 MHz.

In consideration of a tradeoff between the accuracy and the complexity of the equivalent circuit by using VF models, 4-order approximation is used to model the CM impedance of the motor winding with a corresponding circuit topology shown in Fig. 12. The parameter values of the transfer function for 4-order approximation are given in Table 1 and the component values of the circuit are given

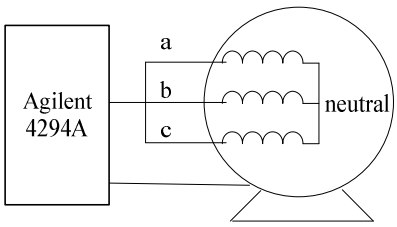

Fig. 11. Schematic for testing Z_{CM}

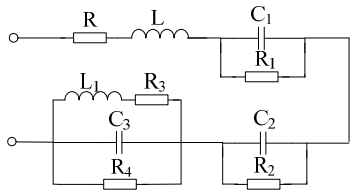

Fig. 12. 4-order VF model

Table 1. Parameter values for 4-order transfer function

d	e
3.2617	5.5226×10^{-8}
p_{kr}	r_{kr}
-0.4533×10^{4}	1.0212×10^{8}
-1.4385×10^{8}	-4.3195×10^{8}
p_{kc} & p_{kc}^{*}	r_{kc} & r_{kc}^{*}
$-0.0226\times10^{8}\pm j0.0647\times10^{8}$	$2.2995\times10^{7}\pm j1.3508\times10^{6}$

Table 2. Component values for 4-order CM equivalent

real	R	L		
	3.26	5.52×10^{-8}		
Real poles	R_1	C_1	R_2	C_2
	22527.24	9.79×10^{-9}	-3.01	-2.31×10^{-9}
Complex pole pairs	R_3	L_1	R_4	C_3
	2.06	1.10×10^{-6}	17.43	2.17×10^{-8}

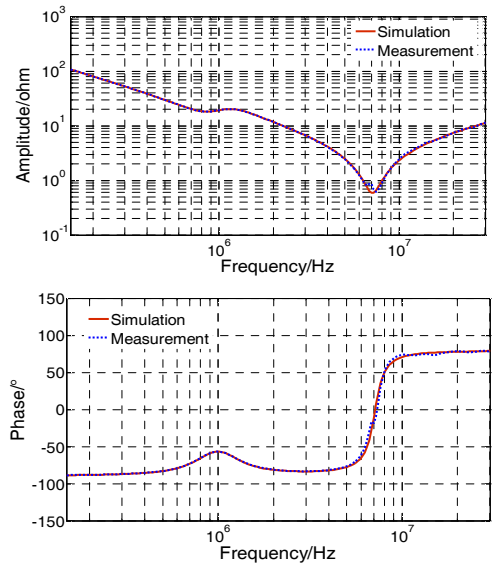

Fig. 13. Measurement and simulation results for motor CM model

in Table 2.

The simulated and experimental results of CM impedance are shown in Fig. 13. This curve shows that the Z_{CM} impedance is almost capacitive when the frequency is below 6 MHz. when the frequency is increasing, the antiresonance occur at the frequency point 7 MHz as the phase angle at this point is 0° and the impedance behaviour is changing from capacitive to inductive. The comparisons of magnitude and phase date shows that the simulation results of 4-order equivalent circuit match the experimental results well in the entire bandwidth for both the magnitude and phase of the Z_{CM}.

4. Model Simulation and Experimental Verification

4.1 EMI simulation

The CM simulation model of the motor drive system is shown in Fig. 14(a). Where Z_{LISN} represents the LISN module; the inverter module is consist of the CM excitation source and parasitic capacitance between the semi-conductors and heat sink; the models of the power line and PMSM are characterized by $Z_{Power\ line}$ and Z_{Motor}, respectively.

All the circuit modules are incorporated into the circuit simulation software and the detailed circuit simulation model of the motor drive system for CM EMI level is shown in Fig. 14(b). The transient emulation type has been selected and simulation computing time is 200 μs with simulation step size 0.1 ns. The CM conducted emission voltage V_{LISN} and current I_{CM} would be simulated and calculated to compare with the results measured on the

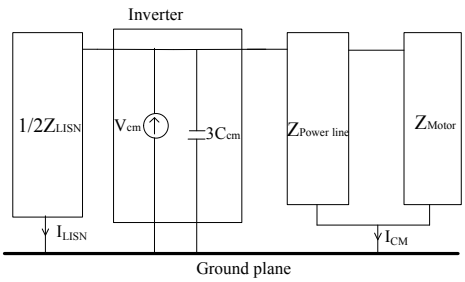

(a) Schematic of the CM EMI model of the motor drive system

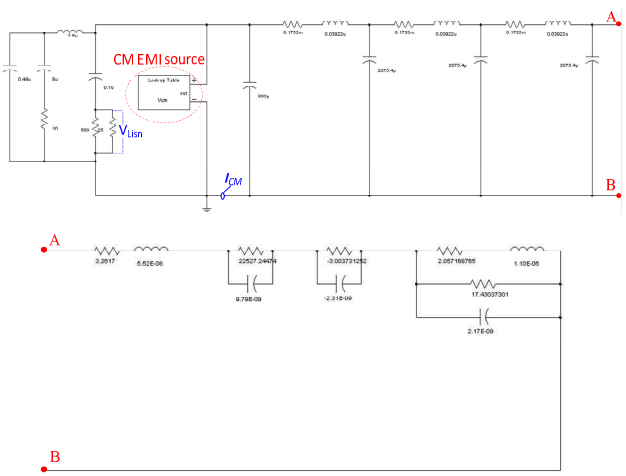

(b) EMI circuit simulation diagram of the motor drive system

Fig. 14. EMI CM model simulation of a motor drive system

experimental bench. Where V_{LISN} can be expressed as:

$$V_{LISN} = 25 \ I_{LISN} \tag{24}$$

4.2 EMI measurement

To validate the effectiveness of the EMI models proposed in this paper, we establish the experimental measurement platform of the motor drive system used in EVs. The setup of the experimental facilities is shown in Figs. 15(a) and (b).

To simulate the actual mounting structures of the motor drive system in a car, the converter case is connected to the car body, which is replaced by the ground plane in the experimental platform. The ground plane comprises a galvanized steel plain sheet with a thickness of 1.2 mm, an area of 2400mm × 1000 mm, and a height of 1000 mm from the ground. Traction battery, as the DC power supply, is connected to the input terminal of $LISN_1$ and output terminal of this device is connected to inverter. The PMSM (45kW) motor was fed by a three-phase voltage-source inverter through a 3-m shielded power line. The driving circuit of the inverter is power by a 12V battery through $LISN_2$ connection to reduce the interference generated by the 12V battery; the start and end of inverter operation is controlled by the host computer through the CAN highway. Current have been measured using a FCC F-33-1 current probe (bandwidth=10 kHz-250 MHz) and the common mode EMI voltage V_{LISN} is obtained as:

$$V_{LISN} = (V_1 + V_2)/2 \tag{25}$$

Where V_1 and V_2 are, respectively, the voltages measured at the terminals of the $LISN_1$.

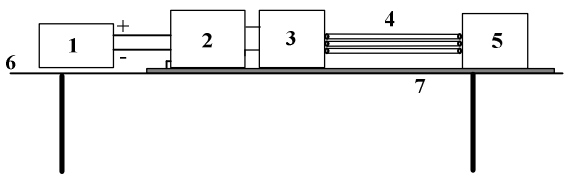

(a) side view

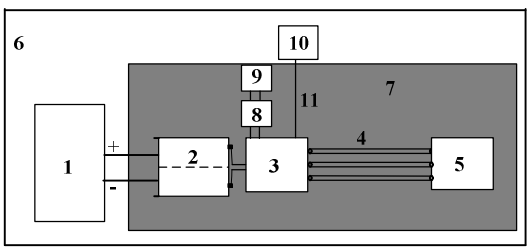

(b) top view

1–traction battery 320 V, 2–$LISN_1$, 3–inverter, 4–power line, 5–PMSM, 6–test stand, 7–ground plane, 8–$LISN_2$, 9–12 V storage battery, 10–computer, 11–CAN highway

Fig. 15. Experiment setup for the motor drive system

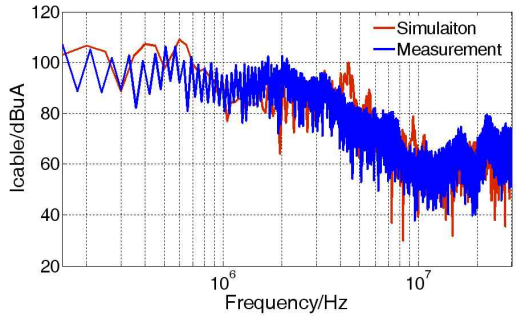

(a) CM current in the ground motor wire

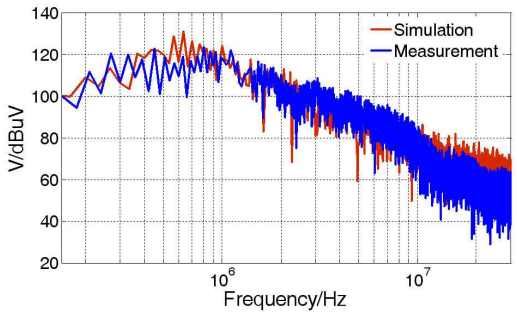

(b) CM voltage on the LISN

Fig. 16. Comparison between measurement and calculation

The simulated and experimental common mode current in the power line shielding layer and motor chassis are presented in Fig. 16(a). Discrepancies between the simulation and experimental results are observed at some frequency ranges, such as 4 MHz to 5 MHz, with an error greater than 10 dB. However, the comparison of the simulation and measurement results indicates good conformance with errors less than 10 dB in the most of the frequency ranges. Therefore, the comparison results show the validity of the proposed power line model and motor model in CM conducted emission.

Fig. 16(b) shows the simulated and the measured results of CM conducted EMI at the terminal of the LISN ports. The comparison of the results in the range 750 kHz to 20 MHz indicates performance that corresponds to errors less than 5 dB, and the difference between the simulation and experimental results are observed at some frequency ranges, with an error no more than 10 dB. Therefore, the comparison results show the good behavior of the proposed inverter and LISN CM models.

These curves show that all impedances and CM source are accurately determined and our method is efficient in predicting CM conducted EMI for the motor drive system.

5. Conclusion

A pragmatic methodology is described in the paper to predict the CM conducted perturbation in a motor drive

system of EVs. An equivalent circuit model has been proposed based on a representation of the full system. The model is reduced to the only described propagation, largely responsible for the major disturbances generated by these devices. Minimizing the complexity of the model make model easy to establish. The processing methods for the inverter consist of two steps: the CM voltage source is obtained by concentrating the output voltage waveform of each leg as one waveform; the stray capacitance has been identified by measurement. The CM model of the power lines based on transmission line model is used and the parameter extraction method in the model combines analytical method and FEM. The processing methods focuses on the motor CM parameters in the prediction model, establishes a high-frequency equivalent circuit model with high accuracy from 150 kHz to 30 MHz based on VF technique. The simulation and measurement results proved that the proposed model effectively describes the CM EMI levels of the motor drive system. The obtained model of the system would be used to design a CM filter for the reduction of conducted CM interference in EVs in future studies. While inserting a CM filter in a modeling such as presented herein, it is possible to design its component to obtain the desired attenuation with actual impedance. Lastly, this method is well matched to represent the CM current flowing in any part of the system: inverter, power line or motor chassis.

Acknowledgements

This work has been supported by the National Natural Science Foundation of China (51177183) and Application Development Planned Program (cstc2013yykfa60001) of Chongqing, China

References

[1] A. Emadi, Y.J. Lee, and K. Rajashekara, "Power electronics and motor drives in electric, hybrid electric, and plug-in hybrid EVs," *IEEE Trans. on Industrial Electronic*, vol. 55, no. 6, pp. 2237-2245, Jun. 2008

[2] M. Ehsani, Y.M. Gao, and J.M. Miller, "Hybrid EVs: architecture and motor drives," *Proceedings of the IEEE*, vol. 95, no. 4, pp. 719-728, Apr. 2007

[3] G. Nanda, and N.C. Kar, "A survey and comparison of characteristics of motor drives used in EVs," *Canadian Conference on Electrical and Computer Engineering*, pp. 811-814, Ottawa, May 2006

[4] D.B. Jay Erdman, R.J. Kerkman, D. Schlegel, and G. Skibinski, "Bearing currents and their relationship to PWM drives," *IEEE Trans. on Power Electronics*, vol. 12, no. 2, pp. 243-252, Mar. 1997

[5] J.M. Erdman, R.J. Kerkman, D.W. Schlegel, and G.L. Skibinski, "Effect of PWM inverters on AC motor bearing currents and shaft voltages," *IEEE Trans. on Industry Applications*, vol. 32, no. 2, pp. 250-259, Apr. 1996

[6] S.A. Pignari, and A. Orlandi, "Long-cable effects on conducted emissions levels," *IEEE Trans. on Electromagnetic Compatibility*, vol. 45, no. 1, pp. 43-54, Feb. 2003

[7] N. Moutoh, M. Nakanishi, M. Kanesaki, and J. Nakashima, "EMI noise control methods suitable for electric vehicle drive systems," *IEEE Trans. on Electromagnetic Compatibility*, vol. 47, no. 4, pp. 930-937, Nov. 2005

[8] M.C. Di Piazza, A. Ragusa, and G. Vitale, "Common mode EMI propagation in high voltage DC supplied induction motor drives for EVs application," *IEEE International Conference on Electric Machines and Drives*, pp. 647-652, 2009

[9] C. Chen, and X. Xu, "Modeling the conducted EMI emission of an electric vehicle (EV) traction drive," *IEEE International symposium on Electromagnetic Compatibility*, vol.2, pp. 796-801, 1998

[10] Y.H. Lee, and A. Nasiri, "Analysis and modeling of conductive EMI noise of power electronics converters in electric and hybrid EVs," *Proceedings of 23th Annual IEEE Applied Power Electronics Conference and Exposition*, pp. 1952-1957, 2008

[11] K. Jia, G. Bohlin, and R. Thottappillil, "Optimal cable assembly for reducing conducted electro-magnetic interference in the traction system," *IET Electrical Systems in Transportation*, vol. 2, no. 1, pp. 29-37, 2012

[12] L. Wang, C.N. Ho, and J. Jatskevich, "High-frequency modeling of the long-cable-fed induction motor drive system using TLM approach for predicting overvoltage transients," *IEEE Trans. on Power Electronics*, vol. 25, no. 10, pp. 2653-2664, Oct. 2010

[13] M. Moreau, N. Idir, and P.L. Moigne, "Modeling of conducted EMI in adjustable speed drives," *IEEE Trans. on Electromagnetic Compatibility*, vol. 51, no. 3, pp. 665-672, Aug. 2009

[14] V. Ardon, J. Aime, O. Chadebec, E. Clavel, J. Guichon, and E. Vialardi, "EMC modeling of an industrial variable speed drive with an adapted PEEC method," *IEEE Trans. on Magnetics*, vol. 46, no. 8, pp. 2892-2898, Aug. 2010

[15] D. Gallo, C. Landi, and N. Pasquino, "Experimental evaluation of conducted emissions by variable-speed drives under variable operating conditions," *IEEE Trans. on Instrumentation and Measurement*, vol. 57, no. 7 pp. 1350-1356, Jul. 2008

[16] T. Qi, J. Graham, and J. Sun, "Characterization of IGBT modules for system EMI simulation". *Proceedings of 25th Annual IEEE Applied Power Electronics Conference and Exposition*, pp. 2220-2225, 2010

[17] A. Nejadpak, and O.A. Mohammed, "Physics-based modeling of power converters from finite element

electromagnetic field computations," *IEEE Trans. on Magnetics*, vol.49, no.1, pp. 567-576, Jan. 2013
[18] N. Idir, Y. Weens, and J.J. Franchaud, "Skin effect and dielectric loss models of power cables," *IEEE Trans. on Dielectrics and Electrical Insulation*, vol. 16, no. 1, pp. 147-154, Feb. 2009
[19] F. Costa, C. Vollaire, and R. Meuret, "Modeling of conducted common mode perturbations in variable-speed drive systems," *IEEE Trans. on Electromagnetic Compatibility*, vol. 47, no. 4, pp. 1012-1021, Nov. 2005
[20] A. Boglietti, A. Cavagnino, and M. Lazzari, "Experimental high-frequency parameter identification of AC electrical motors," *IEEE Trans. on Industry Applications*, vol.43, no.1, pp. 23-29, Feb. 2007
[21] N. Idir, Y. Weens, and J.J. Franchaud, "High-frequency behavior model of AC motors," *IEEE Trans. on Magnetics*, vol. 45, no. 1, pp. 133-138, Jan. 2009
[22] K. Gulez, and A. A. Adam, "High-frequency CM modeling of permanent magnet synchronous motors," *IEEE Trans. on Electromagnetic Compatibility*, vol. 50, no. 2, pp. 423-426, May. 2008
[23] O.A. Mohammed, and S. Ganu, "FE-circuit coupled model of electric machines for simulation and evaluation of EMI issues in motor drives," *IEEE Trans. on Magnetics*, vol. 46, no. 8, pp. 3389-3392, Aug. 2010
[24] B. Gustavsen, and A. Semlyen, "Rational approximation of frequency domain responses by vector fitting," *IEEE Trans. on Power Delivery*, vol. 14, No. 3, pp. 1052-1061, Jul. 1999

Yong-Ming Yang received a M.Sc. degree and a Ph.D. degree in electrical engineering from Chongqing University, Chongqing City, China, in 1987 and 1999. Since 1987, she has served at Chongqing University as a Lecturer (1988), an Associate Professor (1996) and a Professor (2002). Her current research interests are the preventive diagnostic techniques and on-line monitoring techniques for power equipment.

He-Meng Peng was born in Henan Province, China, in 1989. He received his B.S. degree in electrical engineering from Chongqing University, Chongqing, China, in 2009. He is currently working toward the Ph.D degree at the State Key Laboratory of Power Transmission Equipment & System Security and New Technology, China. He current research interests include vehicle electromagnetic compatibility.

Quan-Di Wang was born in Anhui Province, China, in 1954. She received her Ph.D in Electrical Engineering from Chongqing University, Chongqing, China, in 1998. She is currently a professor at the College of Electrical Engineering, Chongqing University, China. Her main research interests include the simulation and numerical computation of electromagnetic field, and vehicle EMC prediction.